Solar Physics (2006) 233: 233–248
DOI: 10.1007/s11207-006-2065-2 

# THE DECELERATION OF AN INTERPLANETARY TRANSIENT FROM THE SUN TO 5 AU

S. J. TAPPIN
*School of Physics and Astronomy, University of Birmingham, Edgbaston, Birmingham B15 2TT, U.K.*
*(e-mail: sjt@star.sr.bham.ac.uk)*

(Received 21 March 2005; accepted 7 August 2005)

**Abstract.** A CME which was first seen in LASCO is tracked through SMEI and on out to *Ulysses*. These measurements allow us to determine the deceleration and compare different models of the deceleration process. It is found that both a simple "snow plough" model and an aerodynamic drag model predict a much more rapid deceleration in the lower solar wind than is observed. Therefore some driving force is needed over an extended range of distances to account for the motion of the transient. It is conjectured that at least part of this driving force may be provided by one of two low-latitude coronal holes which were close to the site of the CME.

## 1. Introduction

Coronal mass ejections (CMEs) have been recognised for many years (Gosling *et al.*, 1974; Tousey *et al.*, 1974). It was quickly realized that these were the near-Sun manifestations of the disturbances responsible for most of the shocks which are seen in interplanetary space (Sheeley *et al.*, 1985). The plasma signatures of CMEs were recognised beyond 1 AU in data from *Ulysses* (Phillips *et al.*, 1992); these are generally described as "interplanetary CMEs" (ICME) or transient interplanetary disturbances. However despite this little is known about how these transient disturbances propagate through the heliosphere. In particular the processes which decelerate them, and those which act to prevent the deceleration have yet to be fully understood.

Over the last decade many CMEs have been studied using LASCO (Large-Angle Spectrographic Coronagraph) (Brueckner *et al.*, 1995), on board the Solar and Heliospheric Observatory (SOHO). In some cases connections have been made to events seen at *Ulysses* (Funsten *et al.*, 1999). But owing to the large distance between the edge of the LASCO field of view at 30 $R_{\odot}$ and *Ulysses*, and to uncertainties in the actual longitude of the CMEs, these identifications are seldom unambiguous and in any case they can tell us little about the propagation of the transient through interplanetary space.

Events seen by the instruments on the Advanced Composition Explorer (ACE) and/or Wind can more often be identified unambiguously with LASCO CMEs, but in these cases because we are dealing with Earth-directed CMEs the speed

measurements from LASCO are often affected by projection effects which are difficult to determine for any individual event (Cid *et al.*, 2004; Dal Lago *et al.*, 2004; Howard and Tappin, 2005).

More recently the Solar Mass Ejection Imager (SMEI) (Eyles *et al.*, 2003) has allowed us to image transients in the 0.5–1 AU range, and many of these have been associated with LASCO CMEs (Tappin *et al.*, 2004; Jackson *et al.*, 2005; Webb *et al.*, in preparation). However to really understand the propagation of transients we need to be able to trace events over as wide a range of heliocentric distance as possible.

In this paper we select a transient that was seen by LASCO, SMEI and by the plasma and magnetometer instruments on *Ulysses* and compare its progress through the heliosphere with that predicted by two simple analytical models for the deceleration of the transient. The models are a "snow-plough" model in which the transient sweeps up the solar wind ahead of it and so continually becomes more massive; and an aerodynamic drag model as proposed by Cargill (2004). We then consider the implications of these comparisons for the driving of CMEs through the corona and lower solar wind.

## 2. The Observations

During the SMEI mission to date, *Ulysses* has been at large distances ($>4.5$ AU) and low latitudes (|heliographic latitude|$<25^\circ$, |ecliptic latitude|$<28^\circ$); thus providing the potential for observations of interplanetary transient disturbances over a large range of heliocentric distances (Tappin, Simnett, and Jackson, 2004). Figure 1 shows some key components of the *Ulysses* trajectory during the first 20 months of SMEI operation. During the intervals from start of normal operations (2003 day 40) to 2003 day 145 and from 2003 day 333 to 2004 day 149 *Ulysses* was in the earthward hemisphere and thus had a reasonable chance of being in the path of transients seen by SMEI. However for much of these intervals, the latitude of *Ulysses* was such that it was in the ranges of position angle poorly seen by SMEI owing to energetic particle and sunlight contamination of the images. As a result of this, out of the original list of 18 suitable SMEI transients presented by Tappin, Simnett, and Jackson (2004) in only one case have we been able to clearly identify the event in both LASCO and *Ulysses*; this was the transient seen by SMEI on 7 April 2003 (day 097), which was identified with an east-limb CME seen by LASCO on 5 April (095). This transient is identified with one of two shocks at *Ulysses*, either that at about 04:45 UT on 18 April (day 108) or that at 16:10 UT on 21 April (day 111).

In LASCO the CME was seen above the east limb (Figure 2), and followed shortly after two slower CMEs more or less to the North–East and the South–West. It first appeared in C3, which covers the range 3.5 to 32 $R_\odot$, in the image

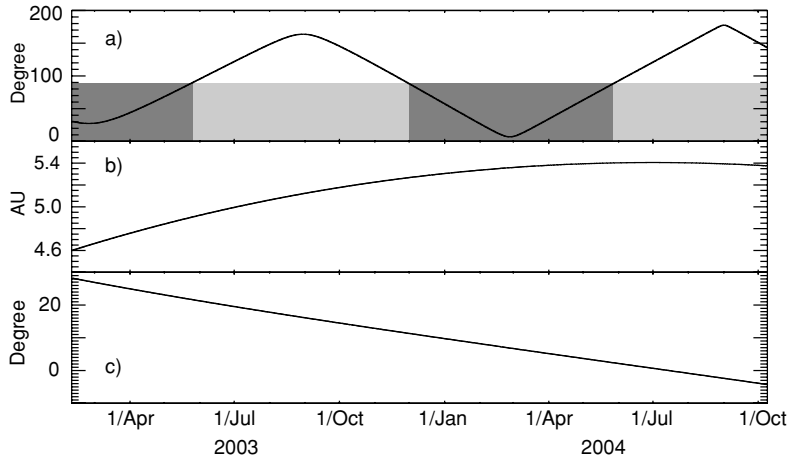


*Figure 1.* The position of *Ulysses* relative to Earth (and thus SMEI and SOHO) from the start of SMEI's operation up to the end of September 2004. (a) The Earth-Sun-*Ulysses* angle, the *dark shading* indicates when *Ulysses* was in the same heliographic hemisphere as Earth, the *light* when *Ulysses* was behind the sky plane, (b) the heliocentric range of *Ulysses*, and (c) the ecliptic latitude of *Ulysses*.

taken at 15:42 UT on 5 April, and had reached the outer edge of the field of view by the image at 20:18 UT. The CME was visible over the heliographic position angle range from 70° to 126°; since at this time the rotation from the heliographic coordinates of LASCO to ecliptic coordinates was about 4°, this corresponds to an ecliptic position angle range of 66–122° (in Figure 2 this 4° rotation has been applied to the LASCO image). The sky-plane speed through C3 was about 1020 km/s.

The Extreme Ultraviolet Imaging Telescope (EIT) (Delaboudinière et al., 1995) observed an eruption starting in the image taken at 14:12 UT. This was centred at a position angle of 108° and about 68° from disk centre, and probably indicates the location of one footpoint of the CME. This suggests that the error in using a sky plane speed from LASCO is at worst 7% ($1 - \sin 68°$).

The details of the instrument and operation of SMEI are described in the instrument (Eyles *et al.*, 2003) and mission (Jackson *et al.*, 2004) papers, so only a brief summary is given here. SMEI was launched on 6 January 2003 into a circular orbit at an altitude of 840 km and an orbital inclination of 98°. This orbit is maintained over the terminator (this is dictated by the WINDSAT instrument with which SMEI shares the Coriolis satellite). SMEI does not take instantaneous images of the sky, but uses three fan-beam cameras each with a field-of-view of approximately $60° \times 4°$ so arranged that in the course of its 102 min orbit an image of almost the entire sky is generated. Like LASCO, SMEI detects thomson-scattered sunlight and thus images electron density. In common with coronagraphs, the intensity observed is a line-of-sight integral of the scattered radiation, with the greatest contribution

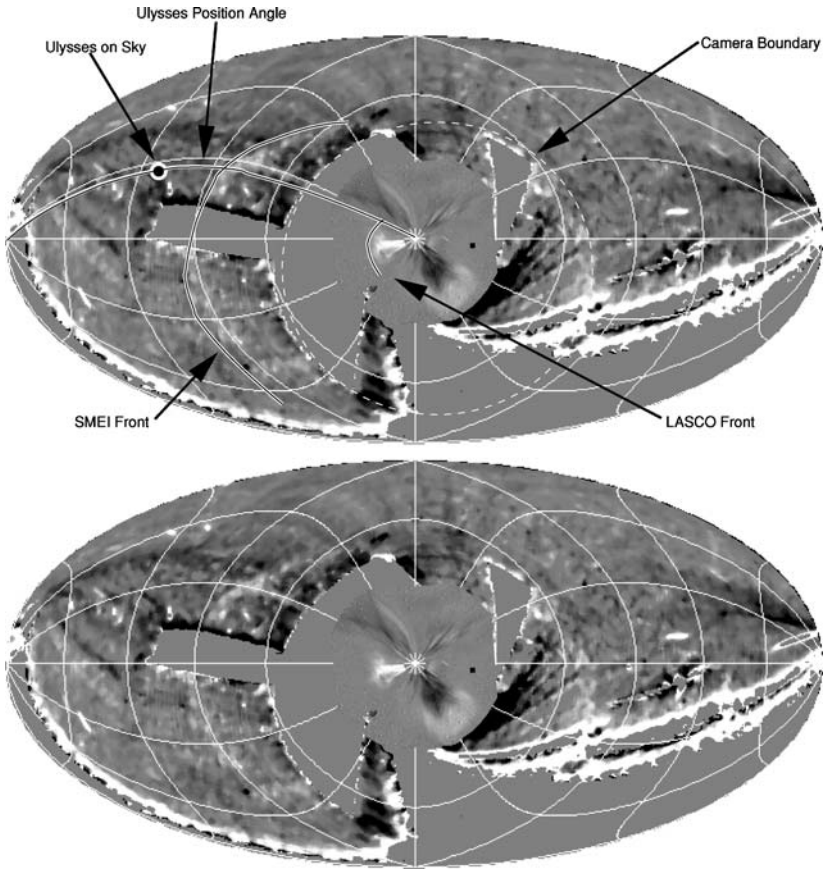


*Figure 2.* Superposed SMEI and LASCO images of the 5–7 April 2003 transient. The *upper panel* has annotations to show the locations of features of interest, the *lower panel* omits these to allow the features to be more easily seen. The SMEI image is an all-sky map in ecliptic coordinates, using the Hammer-Aitoff projection with the Sun at the centre; it covers the orbit from 20:30–22:12 UT on 7 April (Day 97). A background image has been subtracted and a 5 × 5 median has been applied to remove residual stars and other small scale features, the range from black to white is −1.0 to 1.0 in SMEI's internal digitiser units (ADU). The LASCO image was taken at 17:42 UT on 5 April. It is a ratio to an average of 5 pre-event images, with a range from back to white of 0.95–1.05. It has been rotated anti-clockwise by 4° to transform the heliographic orientation of LASCO images to the ecliptic orientation used for SMEI, and is magnified approximately four times compared with the inner regions of the SMEI image. The *arcs* show the locations of the fronts in both images. The position angle and location in the sky of *Ulysses* are also indicated. The *dashed ellipse* shows the boundary between Cameras 2 and 3 in the SMEI image. A grid in elongation and position angle is superposed at 30° intervals on the SMEI image. Note that the brightness seen in the west near the Camera 2 to Camera 3 boundary is not part of the transient, but is a result of variations in stray light levels in Camera 3, with an apparent edge at the transition between Cameras 3 and 2.

coming from the point where the line of sight passes closest to the Sun (the so-called point $p$). Because the elongations are larger for SMEI than for coronagraphs, the scattering is less-strongly peaked towards the point of closest approach. This means that SMEI is reasonably sensitive to disturbances through most of the earthward hemisphere of the solar wind; but it also means that there is greater ambiguity in the interpretation of SMEI images. In order to detect transients in the SMEI images, it is necessary to remove the contribution from stars and the zodiacal light as well as the "quiet" thomson scattering. In the analyses presented here, a 3-day median image has been used to provide this background level.

In SMEI the transient was seen from the orbit covering 12:02–13:44 UT on 7 April (day 97) until that covering 03:16–04:58 UT on 8 April as an apparently slow-moving narrow arc in the North-East (Figure 2). It is however possible to trace the disturbance in the South-Eastern quadrant as well (the transient is much more easily visible in a movie than in still images). Unfortunately the region to the East of the Sun is missing at small elongations as the inner edge of the field of view of the camera looking closest to the Sun was too close to the Sun at this phase of the orbit and sunlight scattering into the camera swamped any useful signal.

The range of position angles covered by the transient in the SMEI images was from about 30° to 150° which is considerably greater than that seen by LASCO. This may be no more than a projection effect (c.f. the interplanetary scintillation simulations of Tappin, 1987), but it may also indicate that the shock ahead of the transient is considerably more extended than the original ejecta. It is also possible that the slow northeastern CME may also be contributing to the apparent extent in the northerly directions. The fact that the leading edge of the transient is seen as a front beyond 90° elongation shows that the transient must be away from the Sun-Earth line (which is confirmed by the lack of a disturbance in the ACE SWEPAM and MAG data). This means that we cannot use the approximation that the line of sight is tangential to the disturbance when the disturbance is close to or beyond the Earth. Height-time profiles for the LASCO and SMEI observations of this transient were generated by manually marking the location of the leading edge of the feature at a position angle close to the projected angle of *Ulysses*. These are shown in Figure 3, the errors in LASCO are very small on the scale of this plot, and the random error in each SMEI elongation measurement is about 2°, which corresponds to about 0.02 AU over the range of elongations covered by the observations and is much smaller than the potential systematic errors from assumptions about the geometry. A sensible speed is obtained on the assumption that the viewing point is about 40° from the Sun-Earth line (using a much greater angle than that implies an unreasonably high speed and requires that the transient be accelerated, while a much smaller angle gives a low speed and deceleration, so that anything outside the range 35–45° is unreasonable). Since we do not see the disturbance inside 50° elongation, we may use the 40° viewing angle for all the SMEI images. The assumption of 40° to the Sun-Earth line gives rise to a speed around 790 km/s through the SMEI field of view and a transit speed from the Sun to ∼1 AU of

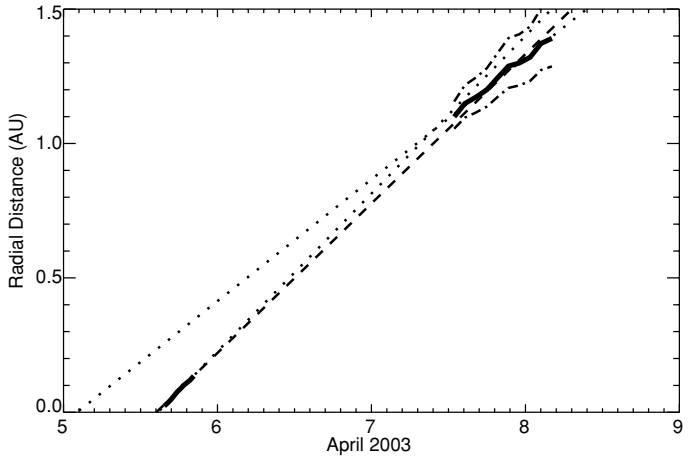


*Figure 3.* The LASCO and SMEI height-time profiles for the 5–7 April 2003 transient. The *heavy lines* show the measured heights, the *dashed line* is the transit speed, while the *dotted lines* are the speeds fitted to the individual components. The *dash-dot lines* indicate the SMEI heights for assumed angles of 35° and 45° to the Sun-Earth line.

around 960 km/s. As can be seen, the profile leaves little room to doubt that the LASCO CME and the SMEI transient are the same event. They also show that there was some deceleration which appears to be concentrated in the higher part of the transit.

The SWOOPS (Bame *et al.*, 1992) and MAG (Balogh *et al.*, 1992) instruments on *Ulysses* detected two shocks either of which could plausibly be related to this event, the first at about 0445 UT on 18 April (day 108) and the second at about 1610 UT on 21 April (day 111) (Figures 4 and 5). At the time of the first of these, *Ulysses* was at a heliocentric range of 4.81 AU, an ecliptic latitude of 23.9°N and an ecliptic longitude 53.9°E of Earth. By the second the distance was 4.82 AU, the latitude 23.7°N and the longitude 56.8°E. Neither shows a clear indication of a magnetic cloud, but since *Ulysses* is probably well towards the flank of the transient this is not that surprising.

A simple-minded calculation of the shock speed based on the assumption that the shock normal is radial i.e. using:

$$v_s = \frac{n_1 v_1 - n_0 v_0}{n_1 - n_0},$$

where $v$ is speed and $n$ is number density and the 0 and 1 subscripts refer to the pre- and post-shock values) gives us speeds of 506 and 492 km/s respectively.

The 18 April shock can be matched to the LASCO and SMEI data by a constant deceleration of about 0.25 m/s$^2$, which also gives a reasonable match to the speed at *Ulysses*. The 21 April shock would require a deceleration of 0.3 m/s$^2$, but that predicts a speed at *Ulysses* that is much slower than observed, and indeed begins to

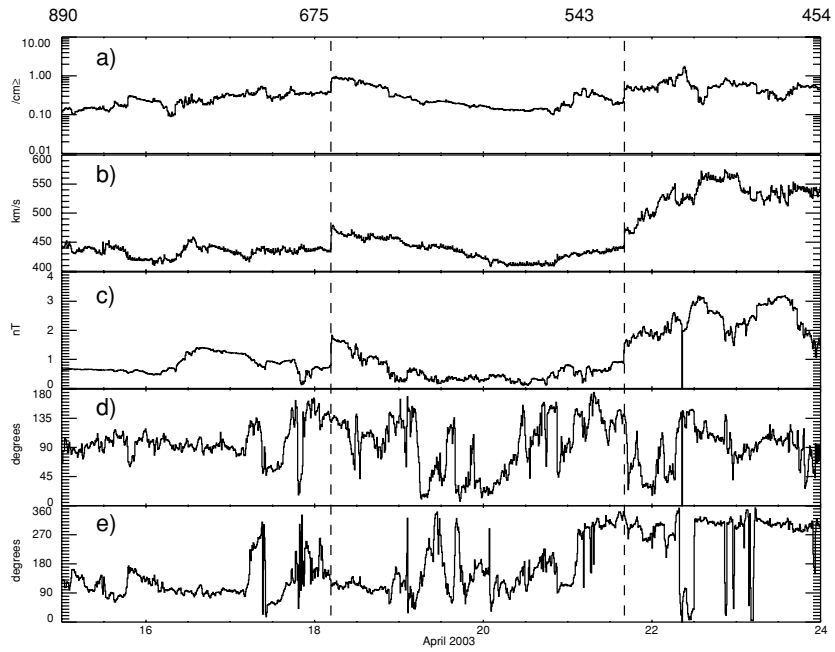


*Figure 4.* Overview of the *Ulysses* plasma and magnetic field observations from 15–23 April 2003. (a) Density, (b) Radial speed, (c) Total Field, (d) Theta (RTN coordinates) and (e) Phi. These are 10-min averages. The *dashed vertical lines* indicate the times of the shocks. The numbers above the plot are mean transit speeds in km/s required from 15:00 UT on 5 April.

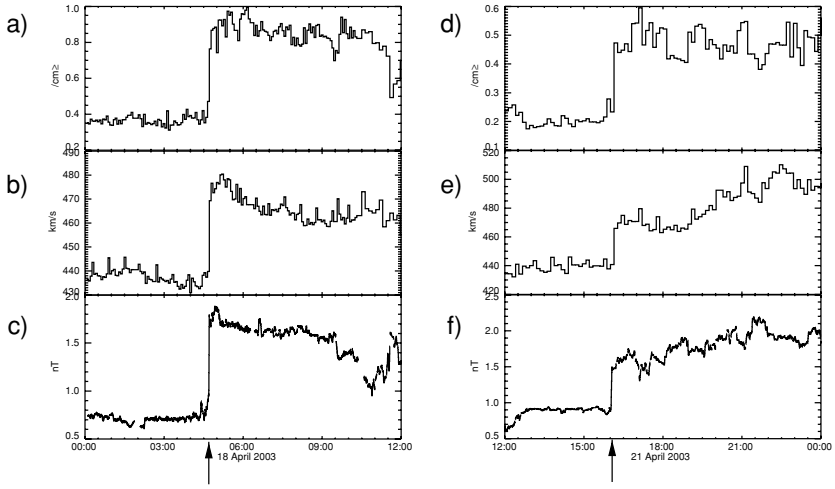


*Figure 5.* Detailed views of the solar wind density, speed and magnetic field magnitude for the two *Ulysses* shocks that could be related to the LASCO/SMEI disturbance under consideration here. (a–c) the 18 April shock (d–f) the 21 April shock (a, d) Ion density (b, e) Radial speed (c, f) Field magnitude. The *arrows* below the *bottom plot* of each column indicate the actual shock arrivals.

fall back soon after reaching *Ulysses*. However, a model with constant deceleration is not physically plausible since any reasonable source of the deceleration of the transient will be related to its speed relative to the solar wind into which it is propagating. In the remainder of this paper we will consider two simple physical models for this deceleration and compare them with the observations.

## 3. Discussion

If we are to understand the propagation of transient disturbances through the heliosphere we must clearly go beyond the simple assumptions of constant deceleration which may be adequate within the LASCO field of view, but are not appropriate to 1 AU and beyond.

Two simple dynamical models can be readily applied:

1. Firstly a simple model in which the transient accretes mass as it propagates and is slowed by the momentum transfer as it accelerates the slower solar wind ahead of it. This is generally described as a "snow plough" model although "bulldozer" might be a more accurate analogy.
2. An aerodynamic drag model such as that by Cargill (2004) in which the transient is decelerated both by sweeping up matter and by the solar wind which it sweeps aside from its path.

The drag model is more physically complete than the snow plough, however it is also more difficult to determine the parameters. Intuitively it would appear that for transients with a large solid angle, the snow plough model may be a reasonable approximation while for smaller disturbances the full drag model would be needed.

### 3.1. The "snow plough" model

Conceptually the "snow plough" model for decelerating interplanetary transients is very simple, being based on the conservation of momentum as the transient sweeps up the slower solar wind ahead of it and accelerates it.

This can easily be shown to give rise to a set of 2 coupled differential equations:

$$\frac{\mathrm{d}^2 r}{\mathrm{d}t^2} = -\frac{\mathrm{d}M}{\mathrm{d}t}\frac{v_c - v_{\mathrm{sw}}}{M}, \tag{1}$$

$$\frac{\mathrm{d}M}{\mathrm{d}t} = \Omega\sigma(v_c - v_{\mathrm{sw}}), \tag{2}$$

where $r$ is the heliocentric range of the transient, $v_c$ is the speed of the transient ($\equiv\frac{\mathrm{d}r}{\mathrm{d}t}$), $v_{\mathrm{sw}}$ is the ambient solar wind speed, $M$ is the mass of the transient, $\Omega$ is its heliocentric solid angle, $\sigma$ is the solar wind sector density (i.e. mass per unit solid angle per unit radial distance $= \rho r^2$, where $\rho$ is the mass density of the solar wind).

We use the sector density and solid angle rather than the more familiar area and mass density as in the case of a CME which is expanding radially into a solar wind with a $1/r^2$ density profile, both are constants.

For the solar wind density inside 1 AU we have used a fit $n = 5r^{-2.45}$ to the coronal/solar wind density tabulations from (Allen, 1976) (which lie within the range determined by Leblanc, Dulk and Bougeret (1998) and we have assumed a $1/r^2$ variation beyond 1 AU to derive the sector density as:

$$\begin{aligned} \sigma(r) &= m_p n_1 r^{-0.45} \quad \text{for } r < 1 \text{ AU} \\ &= m_p n_1 \quad \text{for } r \geq 1 \text{ AU}, \end{aligned}$$

where $m_p$ is the proton mass and $n_1$ is the solar wind number density at 1 AU (taken to be 5 cm$^{-3}$). And thus we get:

$$\begin{aligned} v_{\text{sw}} &= v_1 r^{0.45} \text{ for } \quad r < 1 \text{ AU} \\ &= v_1 \quad \text{for } \quad r \geq 1 \text{ AU}, \end{aligned}$$

where $v_1$ is the solar wind speed at 1 AU (taken to be 440 km/s).

### 3.2. The aerodynamic drag model

The model of CME deceleration by aerodynamical drag processes described by Cargill (2004) was presented in terms of CME area and density, but this formulation can readily be converted to our notation in the form of the differential equation:

$$\frac{\mathrm{d}^2 r}{\mathrm{d}t^2} = -\gamma C_D (v_c - v_{\text{sw}}) |v_c - v_{\text{sw}}|, \tag{3}$$

where $C_D$ is the drag coefficient, and in our coordinate system $\gamma$ (Cargill's Equation (3)) becomes:

$$\gamma = \frac{\sigma \Omega}{M + \frac{\sigma \Omega \Delta r}{2}}, \tag{4}$$

where $\Delta r$ is the radial thickness of the CME. In Cargill (2004) it is stated that for a dense CME $\gamma$ should be a slowly varying function of radial distance, for the purposes of this analysis we have therefore assumed that $\gamma$ is in fact constant. In Equation (4), $M$ is the initial mass of the CME and is constant.

### 3.3. The computations

Both of the models above can be reduced to sets of first-order equations using the identity $v_c \equiv \frac{\mathrm{d}r}{\mathrm{d}t}$. These can then easily be solved numerically given estimates of the speed, mass and solid angle of the CME at the starting height. The initial speed is obtained directly from the LASCO height-time plots.

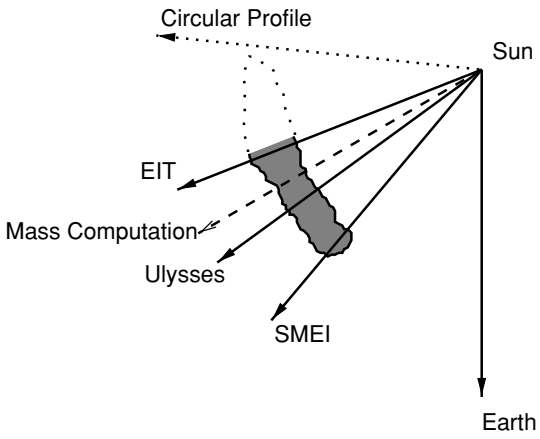


*Figure 6.* The ecliptic projection of the various observations of the transient, indicating the plausible size of the event.

The initial CME mass can be computed from the LASCO images using the theory of Thomson scattering (e.g. Billings, 1966). On the assumption that the CME is at 30° to the plane of the sky, we arrive at an excess mass of $5 \times 10^{12}$ kg for the CME in LASCO C3.

Making an estimate of the solid angle requires an assumption to be made about the size of the CME along the line of sight. We can obtain a lower limit on this by looking at the locations of the various observations of the transient. As is seen in Figure 6 the CME must extend over a range of at least 30° in longitude (i.e. from the near edge as estimated from SMEI to the footpoint location implied by EIT), while the LASCO images show it to have a range of about 55° in latitude. This gives a lower limit of about 0.5 sr for the solid angle, while the assumption of a circular section (longitudinal extent equal to latitudinal) implies a solid angle of about 0.75 sr. For the drag model we assume a thickness of 0.03 AU (6.5 $R_\odot$) at the start and 0.2 AU at *Ulysses* (consistent with the duration and speed of the 18 April disturbance) and a constant drag coefficient of 1.0 (based on Cargill's comparisons with MHD simulations for a dense CME). For a solid angle of 0.5 sr and a thickness of 0.03 AU, we obtain a *total* mass for the CME of $5.8 \times 10^{12}$ kg. In both cases we have started the integration at $20R_\odot$ and continued for 400 hours.

Figure 7 compares the calculated height-time profiles for both models with the observations, in the case of the smallest plausible solid angle for the transient. Both models predict a height-time profile consistent with the second *Ulysses* shock on 21 April, but neither can be reconciled with the SMEI observations which indicate a much faster propagation to near 1 AU than can be obtained from the models. If the CME had a greater solid angle than we have assumed here, then the deceleration would be even greater. To reconcile the model with the SMEI observations would require an order of magnitude increase of mass and while the mass estimate is not

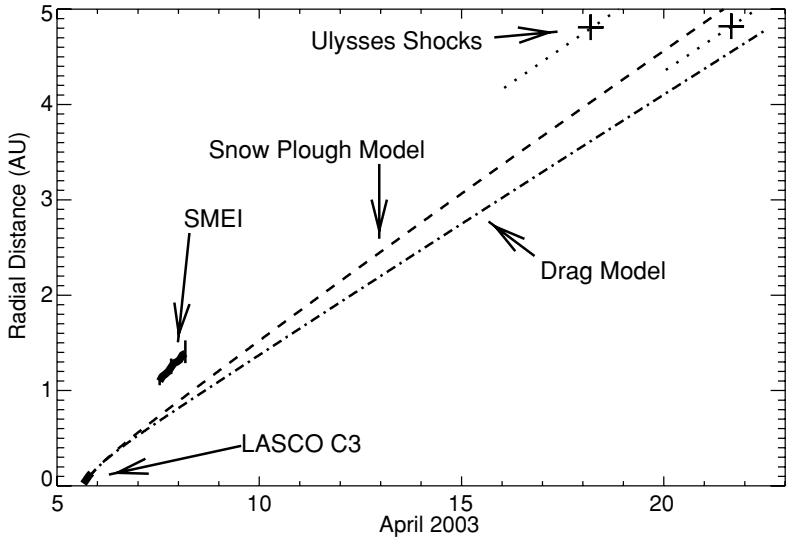


*Figure 7.* The modelled height-time profiles for the transient using the snow plough (*dashed curve*) and aerodynamic drag (*dash-dot curve*) models, on the assumption of a solid angle of 0.5 sr and a speed of 1020 km/s at 20 $R_{\odot}$, compared with the LASCO, SMEI and *Ulysses* observations (*heavy lines and* + *signs*). The *Ulysses* shock speeds are indicated by the *dotted line* segments through their locations.

particularly precise this is unreasonable and would bring the transient to *Ulysses* on 16 April. Therefore we cannot escape the conclusion that some extra source of propulsion for the disturbance must be present over at least a part of its transit to 1 AU. It is also qualitatively evident that if the CME is driven sufficiently to match the SMEI observations, it is not then possible to decelerate it to arrive at *Ulysses* on 21 April as that would require that the transient be decelerated to below the speed at *Ulysses* and then accelerated again, therefore we believe that the 18 April shock must be the one associated with this disturbance. As an aside it should be noted that Cargill (2004) predicts that the value of $\gamma$ in Equation (3) will tend to decrease with distance while we have used a constant, this will tend to bring the two curves closer together.

The 18 April disturbance has a reasonably well-defined density drop at the back edge at 21:03 (the velocity and field are less clear). Taking this as the limit of the disturbance gives a mass of $9 \times 10^{12}$ kg on the assumption of a 0.5 sr solid angle. This is significantly above the initial mass, but well below that predicted by the simple snow plough model at 4.81 AU which is $3 \times 10^{13}$ kg. The implication is that a minimum of 20% of the mass encountered by the transient in propagating to *Ulysses* is swept up by it; however since *Ulysses* appears from Figure 2 to be near the northern limit of the original CME, this is probably a relatively weak lower limit.

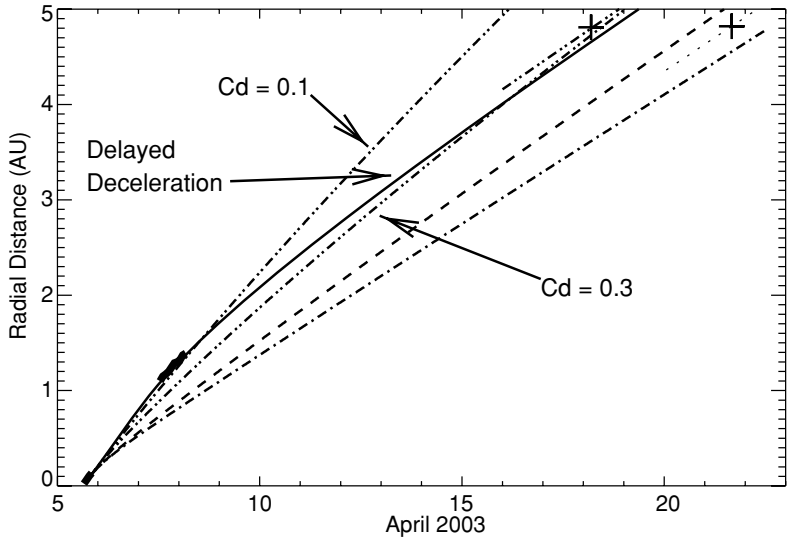


*Figure 8.* As for Figure 7; but with the addition of a model using the drag formulation in which the deceleration is balanced by a driving flow out to 0.8 AU (*solid curve*); and two cases with reduced values of the drag coefficient ($C_D$) *dash-double-dot lines*.

We do not have sufficient coverage or accuracy to allow us to make a realistic estimate of the true form of the driving flow, but if we take a 0.5 sr CME and supply a force balancing the deceleration out to about 0.8 AU and then cut off the driver we get a height-time profile which is in reasonable agreement with the observations from all the instruments (Figure 8).

Alternatively we can try reducing the drag coefficient ($C_D$ in Equation (3)). In this case we find that to match the *Ulysses* shock we require a drag coefficient of around 0.3, and for the SMEI measurements we need only 0.1. These are both far lower than any values found by Cargill (2004) for massive fast CMEs, these profiles are also shown in Figure 8.

What is the source of this driving flow? Long ago (Hewish, Tappin, and Gapper, 1985) postulated that coronal holes were a plausible source of the disturbances seen in interplanetary scintillation observations. Furthermore recent analysis (de Toma *et al.*, 2005) has shown the presence of transient coronal holes following CMEs. The solar wind from a coronal hole is of higher speed and lower density than the ambient, but the momentum flux is conserved (Steinitz and Eyni, 1980). This means that there is an increased energy flux, so the coronal hole can certainly provide some propulsion although whether it is sufficient to account for all of the outward directed force is unclear.

Were there any coronal holes associated with this CME? EIT images following the CME launch show coronal holes behind and ahead of the region of the EIT

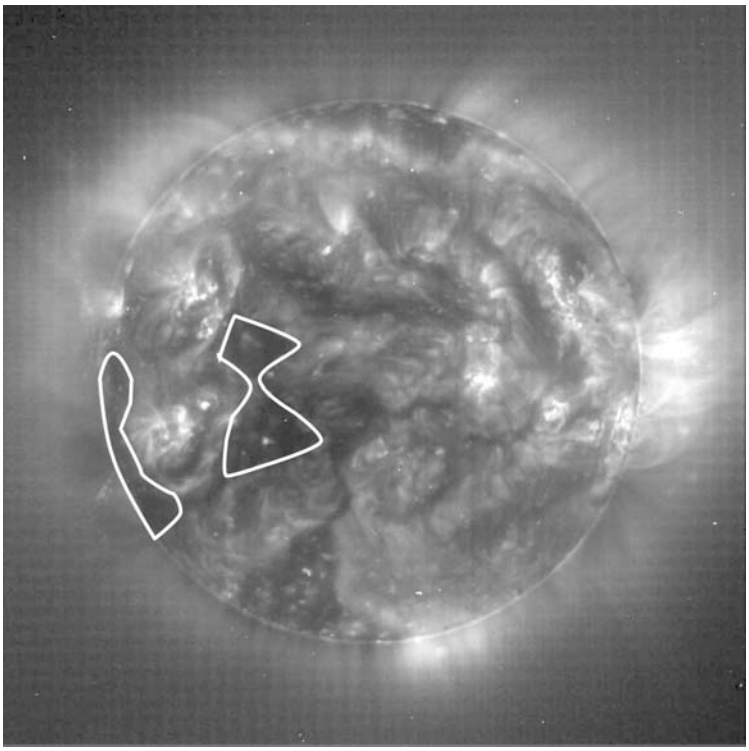

*Figure 9.* An EIT 195 Å image from 01:36 UT on 7 April showing the coronal holes behind and ahead of the region from which the CME emerged. This image is scaled with a cube-root colour mapping.

eruption (Figure 9) which could be the source; however the coronal hole following the EIT eruption would have been very close to the limb at the time of the eruption so it is not possible for us to see whether this hole opened up at the time of the eruption or if it was pre-existing and possibly rotated under the CME. The coronal hole ahead of the region appears to have been largely stable, throughout the interval of interest.

The SWEPAM instrument on ACE (McComas *et al.*, 1998) saw solar wind speeds near Earth rise to 730–750 km/s early on 11 April and on 16 April (Figure 10). These timings are consistent with the coronal holes identified in the EIT images, although the speeds seen at this distance and date are clearly insufficient to provide propulsion to a 1000 km/s CME. However the speed at 1 AU, almost a week after the CME is not necessarily a good indication of what was happening soon after the CME and near the Sun. Overall it seems possible that at least some of the force which propelled the transient out towards 1 AU emanated from one of the coronal holes which surrounded the site of the EIT eruption.

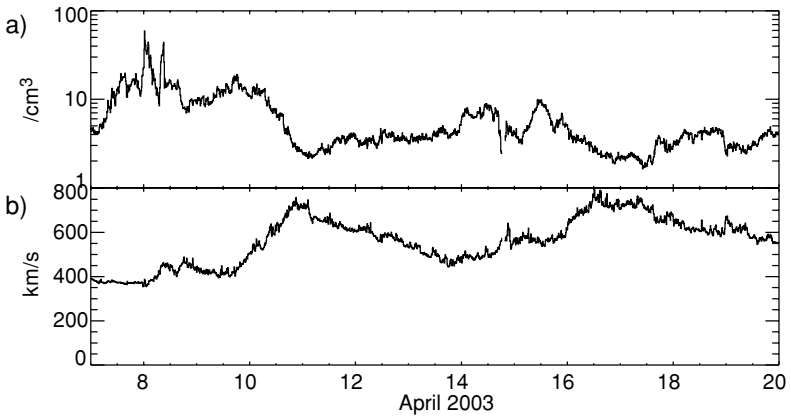


*Figure 10.* ACE plasma measurements following the time of the 5 April transient. (a) Proton density, (b) Solar wind speed.

An alternative source of propulsion via the Lorentz force has been proposed by Chen (1996). More detailed analysis than can be accommodated in this paper would be required to determine whether this force is consistent with the observations.

## 4. Conclusions

We have shown that it is possible to trace an interplanetary disturbance all the way from the Sun to near 5 AU. We have been able to compare its height with simple dynamical models and to show that the deceleration predicted by drag effects is much greater than we observe. We therefore conclude that in order to match the heights seen by the three instruments there must be a driving force opposing the deceleration which probably persists for at least a substantial fraction of 1 AU. We have shown that coronal holes existed which were potentially able to provide the driving force.

In order to more fully understand the propagation of transient disturbances in to the heliosphere beyond 1 AU there is a need for (magneto-)hydrodynamic modelling of the behaviour of CMEs of large solid angle. Fluid simulations will also most probably be needed to determine whether the fast outflow from coronal holes is sufficient to provide the driving force required to overcome the deceleration of the transient by the matter ahead of it.

The later part of the current (late 2004–mid 2005) phase of *Ulysses* being in the forward hemisphere will have *Ulysses* in SMEI's more favoured south-eastern quadrant, offering the possibility of more disturbances being traced through LASCO, SMEI and *Ulysses*.

## Acknowledgements

The author wishes to thank his colleagues on the SMEI and LASCO teams for their support and encouragement; Dr I.R. Stevens for valuable pointers in creating the formulation of the snow plough deceleration model; and Prof. G.M. Simnett, Dr T.A. Howard and Dr I.M Robinson for other valuable discussions and comments on the manuscript. The *Ulysses* plasma and magnetic field data come from ESA's *Ulysses* Data System archive (*http://helio2.estec.esa.nl/ulysses*) and are provided by the instrument teams (SWOOPS, P.I. D.J. McComas and MAG, P.I. A. Balogh). The ACE plasma data are provided by the ACE/SWEPAM team and obtained from the ACE Science Center (*http://www.srl.caltech.edu/ACE/ASC/*). SOHO and *Ulysses* are both projects of international cooperation between NASA and ESA. SMEI is a collaborative project of the U.S. Air Force Research Laboratory, the University of Birmingham, U.K., NASA, the University of California at San Diego, and Boston College. Financial support has been provided by the Air Force, the University of Birmingham, and NASA. The author also thanks the referee for some clarifications regarding the aerodynamic drag deceleration model.

## References

Allen, C. W.: 1976, *Astrophysical Quantities*, (3rd edition), Athlone Press, London.

Balogh, A., Beek, T. J., Forsyth, R. J., Hedgecock, P. C., Marquedant, R. J., Smith, E. J., Southwood, D. J., and Tsurutani, B. T.: 1992, *Astron. Astrophys. Suppl.* **92**, 221.

Bame, S. J., McComas, D. J., Barraclough, B. L., Phillips, J. L., Sofaly, K. J., Chavez, J. C., Goldstein, B. E., and Sakurai, R. K.: 1992, *Astron. Astrophys. Suppl.* **92**, 237.

Billings, D. E.: 1966, *A Guide to the Solar Corona*, Academic Press, New York.

Brueckner, G. E., Howard, R. A., Koomen, M. J., Korendyke, C. M., Michels, D. J., Moses, J. D., Socker, D. G., Dere, K. P., Lamy, P. L., Llebaria, A., Bout, M. V., Schwenn, R., Simnett, G. M., Bedford, D. K., and Eyles, C. J.: 1995, *Solar Phys.* **162**, 357.

Cargill, P. J.: 2004, *Solar Phys.* **221**, 135.

Chen, J.: 1996, *J. Geophys. Res.* **101**, 27499.

Cid, C., Hidalgo, M. A., Saiz, E., Cerrato, Y., and Sequeiros, J.: 2004, *Solar Phys.* **223**, 231.

Dal Lago, A., Vieira, L. E. A., Echer, E., Gonzalez, W. D., de Gonzalez, A. L. C., Guarnieri, F. L., Schuch, N. J., and Schwenn, R.: 2004, *Solar Phys.* **222**, 323.

Delaboudinière, J.-P., Artzner, G. E., Brunaud, J., Gabriel, A. H., Hochedez, J. F., Millier, F., Song, X. Y., Au, B., Dere, K. P., Howard, R. A., Kreplin, R., Michels, D. J., Moses, J. D., Defise, J. M., Jamar, C., Rochus, P., Chauvineau, J. P., Marioge, J. P., Catura, R. C., Lemen, J. R., Shing, L., Stern, R. A., Gurman, J. B., Neupert, W. M., Maucherat, A., Clette, F., Cugnon, P., and van Dessel, E. L.: 1995, *Solar Phys.* **162**, 291.

de Toma, G., Holtzer, T. E., Burkepile, J. T., and Gilbert, H. R.: 2005, *Astrophys. J.* **621**, 1109.

Eyles, C. J., Simnett, G. M., Cooke, M. P., Jackson, B. V., Buffington, A., Hick, P. P., Waltham, N. R., King, J. M., Anderson, P. A., and Holladay, P. E.: 2003, *Solar Phys.* **217**, 319.

Funsten, H. O., Gosling, J. T., Riley, P., St. Cyr, O. C., Forsyth, R. J., Howard, R. A., and Schwenn, R.: 1999, *J. Geophys. Res.* **104**, 6679.

Gosling, J. T., Hildner, E., MacQueen, R. M., Munro, R. H., Poland, A. I., and Ross, C. L.: 1974, *J. Geophys. Res.* **79**, 4581.
Hewish, A., Tappin, S. J., and Gapper, G. R.: 1985, *Nature* **341**, 137.
Howard, T. A. and Tappin, S. J.: 2005, *Astron. Astrophys.* **440**, 373.
Jackson, B. V., Buffington, A., Hick, P. P., Altrock, R. C., Figueroa, S., Holladay, P. E., Johnston, J. C., Kahler, S. W., Mozer, J. B., Price, S., Radick, R. R., Sagalyn, R., Sinclair, D., Simnett, G. M., Eyles, C. J., Cooke, M. P., Tappin S. J., Kuchar, T., Mizuno, D., Webb, D. F., Anderson, P. A., Keil, S. L., Gold, R. E., and Waltham, N.R.: 2004, *Solar Phys.* **225**, 177.
Jackson, B. V., Buffington, A., Hick, P. P., Wang, X., and Webb, D.: 2005, *J. Geophys. Res.*, submitted.
Leblanc, Y., Dulk, G. A., and Bougeret, J.-L.: 1998, *Solar Phys.* **183**, 165.
McComas, D. J., Bame, S. J., Barker, P., Feldman, W. C., Phillips, J. L., Riley, P., and Griffee, J. W.: 1998, *Space Sci. Rev.* **86**, 563.
Phillips, J. L., Bame, S. J., Gosling, J. T., McComas, D. J., Goldstein, B. E., Smith, E. J., Balogh, A., and Forsyth, R. J.: 1992, *Geophys. Res. Lett.* **19**, 1239.
Sheeley, N. R., Jr., Howard, R. A., Michels, D. J., Koomen, M. J., Schwenn, R., Muehlhaeuser, K. H., and Rosenbauer, H.: 1985, *J. Geophys. Res.* **90**, 163.
Steinitz, R. and Eyni, M.: 1980, *Astrophys. J.* **241**, 417.
Tappin, S. J.: 1987, *Planet. Space Sci.* **35**, 271.
Tappin, J., Simnett, G. M., and Jackson, B. V.: 2004, American Geophysical Union, Fall Meeting 2004, abstract #SH21A-0394.
Tappin, S. J., Buffington, A., Cooke, M. P., Eyles, C. J., Hick, P. P., Holladay, P. E., Jackson, B. V., Johnston, J. C., Kuchar, T., Mizuno, D., Mozer, J. B., Price, S., Radick, R. R., Simnett, G. M., Sinclair, D., Waltham, N. R., and Webb, D. F.: 2004, *Geophys. Res. Lett.* **31**, Cite id L02802.
Tousey, R., Howard, R. A., and Koomen, M. J.: 1974, *Bull. Am. Astron Soc.* **6**, 295.